Research Square

Preprints are preliminary reports that have not undergone peer review.
They should not be considered conclusive, used to inform clinical practice,
or referenced by the media as validated information.

Voxel-wise Radiomics Habitat Modeling of Multiparametric Magnetic Resonance Imaging for Isocitrate Dehydrogenase Status Prediction and Survival Stratification in Diffuse Glioma

Tao Zheng
The First Hospital of Qinhuangdao
Linsha Yang
The First Hospital of Qinhuangdao
Duo Zhang
Baoding No. 1 Central Hospital
Juan Du
The First Hospital of Qinhuangdao
Qinglei Shi
School of Medicine, Chinese University of Hong Kong (Shenzhen) & Shenzhen Research Institute of Big Data
Defeng Liu
defengliu2023@163.com
The First Hospital of Qinhuangdao

Research Article

Keywords: Gliomas, Multiparametric MRI, Voxel-wise Analysis, Radiomics, IDH Status

Posted Date: August 24th, 2026

DOI: https://doi.org/10.21203/rs.3.rs-10620328/v1

License: This work is licensed under a Creative Commons Attribution 4.0 International License.
Read Full License

Additional Declarations: No competing interests reported.

Voxel-wise Radiomics Habitat Modeling of Multiparametric Magnetic Resonance Imaging for Isocitrate Dehydrogenase Status Prediction and Survival Stratification in Diffuse Glioma

Abstract

Purpose: To develop and externally validate a voxel-wise probabilistic multiparametric MRI habitat framework for preoperative isocitrate dehydrogenase classification in diffuse glioma and to explore its association with overall survival.

Material and Methods: This retrospective multicenter study included 269 adults with pathologically confirmed diffuse glioma, comprising 174 training and 95 external-validation patients. Preoperative MRI included contrast-enhanced T1-weighted, T2-weighted, T2-weighted fluid-attenuated inversion recovery, apparent diffusion coefficient, and cerebral blood flow images. Tumor and peritumoral edema were segmented using nnU-Net v2. Sliding-window radiomics generated voxel-wise feature maps, and Gaussian mixture models constructed probabilistic habitats. Habitat metrics, tumor–edema differential features, and clinical variables were used for IDH classification. Exploratory survival analysis used a separate imaging-only signature derived from 13 retained imaging predictors and evaluated by Kaplan–Meier and Cox regression analyses.

Results: The imaging-only habitat model (TEΔ-ALL) achieved an external-validation an area under the receiver operating characteristic curve of 0.921. The combined clinical–imaging model (Clin+TEΔ-ALL) achieved the highest discrimination (AUC, 0.955; 95% CI, 0.905–0.989), outperforming the clinical-only model (AUC, 0.660),

with favorable calibration and greater net benefit. SHAP identified perfusion- and diffusion-related entropy metrics as major contributors. In the external survival cohort, the imaging-only signature stratified overall survival (log-rank $P < 0.0001$) and remained independently associated with survival after adjustment (hazard ratio, 4.225 per standard-deviation increase; 95% CI, 2.355–7.580; $P < 0.001$).

Conclusion: Voxel-wise probabilistic MRI habitat modeling captured spatial tumor heterogeneity and showed potential for noninvasive IDH assessment and survival risk stratification in glioma.

Keywords

Gliomas, Multiparametric MRI, Voxel-wise Analysis, Radiomics, IDH Status

1 Introduction

Isocitrate dehydrogenase (IDH) status is central to the molecular classification, risk stratification, and treatment planning of diffuse glioma [1-4]. Although IDH status is determined by histopathology and genetic testing, preoperative noninvasive assessment may support surgical planning, biopsy targeting, treatment selection, and patient counseling, particularly because tissue sampling can be affected by spatial tumor heterogeneity [5].

Conventional MRI-based radiomics and deep learning have shown promise for IDH prediction by extracting quantitative features from structural, diffusion, and perfusion MRI [6-11]. However, most approaches summarize the tumor as a single region of interest using global intensity, shape, or texture descriptors. Such region-level representations may overlook spatially distinct subregions within the tumor and

peritumoral edema, thereby underrepresenting intratumoral and peritumoral ecological heterogeneity.

Habitat imaging has emerged as a strategy for characterizing spatial tumor heterogeneity by partitioning tumors into imaging phenotypes that may reflect differences in cellularity, perfusion, edema, angiogenesis, and microenvironmental gradients [12-14]. This approach is particularly relevant in glioma, where IDH-related biology is linked to vascular remodeling, infiltrative growth, and microenvironmental alterations. However, conventional habitat methods often rely on hard clustering or region-level summaries, which may compress continuous spatial information and produce variable label meanings across patients, limiting interpretability and comparability [15].

Voxel-wise radiomics habitat modeling addresses these limitations by extracting local texture features around each voxel and modeling habitat membership probabilistically [16]. This strategy may better capture transitional tissue states and spatially continuous microenvironmental variation. We therefore hypothesized that probabilistic voxel-wise habitat metrics derived from multiparametric MRI could improve preoperative IDH classification and provide prognostic information beyond routine clinical variables.

The aim of this study was to develop and externally validate a multicenter voxel-wise probabilistic radiomics habitat framework using structural, diffusion, and perfusion MRI for IDH status assessment and overall survival risk stratification in glioma.

2 Materials and Methods

2.1 Study design and patients

This retrospective study included consecutive adults with diffuse glioma treated at two tertiary hospitals from January 2016 to December 2025. Inclusion criteria were age ≥18 years, histopathologically confirmed diffuse glioma after resection or stereotactic biopsy, complete preoperative multiparametric MRI within 2 weeks before surgery, and available clinical and molecular data. Exclusion criteria were prior treatment before MRI, severe imaging artifacts or major protocol inconsistency, and missing or indeterminate IDH testing. Of 297 initially identified patients, 269 were included: 174 from Center A for training and 95 from Center B for external validation. The selection process is shown in Supplementary Figure S1.

Histopathological and molecular diagnoses were assigned according to the 2021 World Health Organization Classification of Tumors of the Central Nervous System, fifth edition (WHO CNS5) [17]. Integrated diagnoses included astrocytoma, IDH-mutant; oligodendroglioma, IDH-mutant and 1p/19q-codeleted; and glioblastoma, IDH-wildtype. CNS WHO grade was recorded accordingly. IDH status was initially assessed using IDH1 R132H immunohistochemistry. Among immunohistochemistry-negative cases, 126 underwent Sanger sequencing and 85 underwent next-generation sequencing for non-canonical IDH1/2 mutations; 7 were reclassified as IDH-mutant and 204 were confirmed as IDH-wildtype.

Clinical variables included age, sex, WHO CNS5 integrated diagnosis, and tumor location. Location was assigned by registering tumor masks to MNI152 space and determining overlap with atlas-defined regions; tumors involving two or more lobes were categorized as multilobar. The Ethics Committee of XXX Hospital approved the

study (2023KZ065; May 17, 2023) and waived informed consent. All procedures complied with the Declaration of Helsinki. The workflow is shown in Figure 1.

2.2 MRI preprocessing and segmentation

All patients underwent preoperative MRI on 1.5-T or 3.0-T Siemens, GE, or Philips scanners. Sequences included contrast-enhanced T1-weighted imaging (T1CE), T2-weighted imaging (T2WI), T2-FLAIR, diffusion-weighted imaging with apparent diffusion coefficient (ADC) maps, and arterial spin labeling-derived cerebral blood flow (CBF) maps (Supplementary Table S1).

Preprocessing used SimpleITK and ANTsPy. Structural images underwent N4 bias correction. All modalities were rigidly registered to T1CE space, visually inspected, resampled to $1 \times 1 \times 1$ mm³, skull-stripped using HD-BET [18] , and z-score normalized within brain parenchyma. Masks were resampled using nearest-neighbor interpolation. Tumor core and peritumoral edema were automatically segmented using nnU-Net v2 with the 3D full-resolution configuration trained on BraTS 2021 data, followed by visual quality inspection [19].

2.3 Voxel-wise Feature Mapping

Voxel-wise radiomics maps were generated using a three-dimensional sliding-window strategy. For each voxel within the tumor core and edema, local features were calculated from a $7 \times 7 \times 7$ voxel neighborhood, using only voxels inside the mask at segmentation boundaries. Features were extracted independently for each modality using a customized PyRadiomics-based pipeline and mapped back to MRI space. In total, 33 voxel-wise radiomics features were extracted per modality (Supplementary Methods

S1). The pipeline is publicly available at https://github.com/zt3226073/radiomics-habitat-pipeline.

Voxel-wise habitat modeling was performed separately for each modality using diagonal-covariance Gaussian mixture models. Feature vectors from the tumor and edema regions generated posterior probability maps of habitat membership. The number of habitats was selected in the training set using the Bayesian information criterion across K = 2–8. To prevent information leakage, model parameters were estimated only from training data and fixed for external validation.

Because habitat labels were not assumed directly comparable across patients, label-independent patient-level metrics were extracted from the probability maps, including habitat entropy, dominance ratio, effective habitat number, Moran's I, fragmentation index, and Gini coefficient. This approach avoided assigning fixed biological meanings to arbitrary cluster labels and improved comparability across patients. Tumor–edema differential features (Δ), including Δentropy, ΔMoran's I, and Δfragmentation index, quantified spatial differences between the tumor core and peritumoral edema (Supplementary Methods S2 and S3).

2.4 IDH Prediction Modeling

After z-score standardization, ComBat harmonization reduced scanner-related batch effects, with scanner model as the batch variable and the largest training scanner group as reference (Supplementary Methods S4) [20]. IDH status and other outcomes were not included during harmonization, and external validation features were mapped to the training-defined reference distribution.

Clinical variables available before surgery included age, sex, and tumor location. WHO CNS5 integrated diagnosis and CNS WHO grade were recorded for cohort characterization but excluded from feature selection and IDH models because they were determined after tissue diagnosis and incorporated IDH-related information. The primary clinical–imaging model, Clin+TEΔ-ALL, used prespecified preoperative clinical variables and habitat features from tumor, peritumoral edema, and matched tumor–edema differences across all MRI modalities. Elastic Net retained 13 imaging predictors together with age and tumor location, whereas sex was not retained. To evaluate spatial compartment and modality contributions within a common selected-feature framework, nested feature-subset ablation models used corresponding subsets of the 13 retained imaging predictors. The TEΔ-ALL model included all retained imaging predictors but excluded clinical variables; T-ALL and E-ALL included only retained tumor- and edema-region predictors, respectively; and TE-ALL combined retained tumor- and edema-region predictors without tumor–edema differential features. Modality-specific models comprised TE-FUNC, TEΔ-FUNC, TE-STRUCT, and TEΔ-STRUCT. These comparator models therefore represented feature-subset ablations of Clin+TEΔ-ALL rather than independently selected models.

In this nomenclature, T denotes tumor-region features, E denotes edema-region features, TE denotes the combination of tumor- and edema-region features, and TEΔ denotes the combination of tumor-region, edema-region, and tumor–edema differential features. ALL denotes all MRI modalities; FUNC denotes functional modalities comprising ADC and CBF; STRUCT denotes structural modalities comprising T1CE, T2WI, and

T2-FLAIR; and Clin+ indicates the addition of retained clinical predictors. Candidate classifiers included logistic regression, random forest, support vector machine, XGBoost, multilayer perceptron, and decision tree. Classifier selection and hyperparameter optimization were performed using Optuna with the Tree-structured Parzen Estimator algorithm, with cross-validated AUC as the objective function [21]. All model development used nested stratified five-fold cross-validation in the training cohort; the external cohort was reserved for final evaluation.

Model performance was evaluated using AUC, accuracy, sensitivity, specificity, and F1max. Operating thresholds were determined in training and applied unchanged to external validation. AUC 95% confidence intervals were estimated using 1,000 bootstrap resamples, and DeLong tests compared models. Calibration was assessed using calibration curves and the Brier score, clinical utility using decision curve analysis, and interpretability using Shapley Additive Explanations (SHAP).

2.5 Survival Analysis

Overall survival was defined from initial diagnosis to death from any cause or last follow-up, with a cutoff date of February 2026. Exploratory survival analysis included external validation patients with available follow-up and complete survival-related clinicopathological and treatment information, including age, sex, location, CNS WHO grade, O6-methylguanine-DNA methyltransferase (MGMT) promoter methylation, Karnofsky Performance Status (KPS), extent of resection (EOR), and standard treatment status. Among 95 external validation patients, 61 met these criteria (Supplementary Methods S5).

For exploratory survival analysis, a separate imaging-only habitat signature was constructed from the same 13 imaging predictors of the TEΔ-ALL model. A logistic regression model was independently refitted in the training cohort, and the resulting scaling parameters and coefficients were applied unchanged to external validation patients (Supplementary Methods S6). Patients were stratified into high- and low-risk groups using the optimal cutoff determined by X-tile software. Kaplan–Meier curves were compared using the log-rank test. Associations with overall survival were evaluated using univariable and multivariable Cox proportional hazards models. Given the limited sample size and event count, the primary model included the imaging-only signature, age, KPS, MGMT status, and EOR. Sensitivity models additionally adjusted for CNS WHO grade or standard treatment. IDH status and WHO CNS5 integrated diagnosis were excluded because the signature was developed for IDH prediction and integrated diagnosis incorporates IDH status; their inclusion could introduce circular adjustment and obscure prognostic information carried by the imaging signature. The analyses evaluated whether the signature was associated with survival after adjustment for available clinical, molecular, surgical, and treatment-related covariates rather than independence from IDH status or integrated diagnosis. This survival analysis was considered exploratory because it was restricted to the external validation subset with complete follow-up and covariate data. Proportional hazards assumptions were assessed using Schoenfeld residuals.

2.6 Statistical Analysis

Analyses were performed in Python. Normality was assessed using the Shapiro–Wilk

test. Normally distributed variables were presented as mean ± standard deviation and compared using independent-samples t tests; nonnormally distributed variables as median and interquartile range and compared using Mann–Whitney U tests. Categorical variables were presented as frequency and percentage and compared using chi-square or Fisher exact tests. All tests were two-sided, and $P < 0.05$ was considered significant.

3 Results

3.1 Patients

The training and external validation sets included 174 and 95 patients, respectively (Table 1). Age, sex, tumor location, CNS WHO grade, and IDH status were similar between sets. IDH-mutant tumors were present in 42 training patients (24.1%) and 23 validation patients (24.2%).

3.2 Feature Selection

Bayesian information criterion analysis supported K = 3 for most MRI sequences and regions; therefore, K = 3 was selected for overall model stability (Supplementary Table S2). After ComBat harmonization, the proportion of habitat metrics with significant scanner-related differences decreased from 62.7% to 9.3% (Supplementary Figures S2 and S3).

Among 75 candidate habitat metrics and prespecified clinical variables, Elastic Net retained 15 predictors for the combined clinical-imaging model: 13 imaging predictors, age, and tumor location. Sex was not retained. The 13 imaging predictors formed the imaging-only signature for exploratory survival analysis; age and location were components only of the combined IDH model (Supplementary Figure S4). Selected

imaging features were mainly derived from ADC and CBF and included tumor, edema, and differential metrics. Logistic regression achieved the best overall performance and was used for subsequent modeling (Supplementary Table S3).

3.3 Model Performance and Comparison

Multiple models evaluated contributions from spatial regions, imaging modalities, and tumor-edema differential features. In external validation, Clin+TEΔ-ALL achieved the best performance, with an AUC of 0.955 (95% CI, 0.905-0.989), compared with 0.660 for the clinical-only model and 0.921 for TEΔ-ALL (Figure 2, Supplementary Table S4, Supplementary Figure S5).

Among habitat models, TEΔ-ALL significantly outperformed TE-ALL (P = 0.046), T-ALL (P = 0.005), and E-ALL (P < 0.001), indicating added information from tumor-edema differential features. TE-ALL also outperformed T-ALL (P = 0.040) and E-ALL (P = 0.018), whereas T-ALL and E-ALL did not differ (P = 0.234).

Functional models showed numerically higher AUCs than structural models, but differences between TEΔ-FUNC and TEΔ-STRUCT (P = 0.322) and between TE-FUNC and TE-STRUCT (P = 0.059) were not significant. TEΔ-ALL significantly outperformed TEΔ-FUNC (P = 0.023), TEΔ-STRUCT (P = 0.010), TE-FUNC (P = 0.012), and TE-STRUCT (P < 0.001), supporting complementary contributions from functional and structural phenotypes. Clin+TEΔ-ALL also outperformed the clinical model (P < 0.001) and TEΔ-ALL (P = 0.039), supporting incremental value from integrating clinical and imaging variables.

3.4 Calibration, clinical utility, and interpretability

In external validation, Clin+TEΔ-ALL showed acceptable calibration, with a Brier score of 0.103 (Figure 3A). Decision curve analysis suggested higher net benefit than clinical-only and imaging-only comparator models across clinically relevant thresholds; uncertainty intervals were not estimated, so these findings were interpreted descriptively rather than as formal evidence of clinical superiority (Figure 3B).

SHAP identified functional habitat features as the main contributors, with CBF_Tumor_habitat_entropy_mean and ADC_Tumor_habitat_entropy_mean ranking highest (Figure 4). Edema and differential metrics, including ΔMoran's I and Δentropy, also contributed. Representative IDH-wildtype gliomas showed greater perfusion- and diffusion-related heterogeneity and fragmentation, whereas IDH-mutant tumors were relatively homogeneous (Figure 5).

3.5 Survival analysis

Among 95 external validation patients, 61 had complete follow-up and survival-related clinicopathological and treatment information. Included and excluded patients showed no significant differences in sex, IDH status, location, or WHO CNS5 integrated diagnosis (Supplementary Table S5).

The same 13 imaging predictors selected for the Clin+TEΔ-ALL model were used in the separately refitted imaging-only model; definitions and coefficients are provided in Supplementary Table S6. X-tile identified a cutoff of -1.046. High-risk patients had significantly poorer overall survival than low-risk patients (log-rank $P < 0.0001$; Figure 6).

In univariable Cox analysis, the signature was associated with overall survival (HR,

4.979 per 1-SD increase; 95% CI, 2.903-8.540; P < 0.001). Age, KPS, MGMT status, and EOR were also associated with survival, whereas sex and location were not (Supplementary Table S7).

In the primary multivariable model, the signature remained independently associated with survival after adjustment for age, KPS, MGMT status, and EOR (HR, 4.225 per 1-SD increase; 95% CI, 2.355-7.580; P < 0.001). This association remained stable after additional adjustment for CNS WHO grade or standard treatment (Supplementary Table S8).

4 Discussion

This study developed and externally validated a voxel-wise probabilistic radiomics habitat framework for noninvasive molecular and prognostic assessment of diffuse glioma. By capturing tumor–edema habitat organization from multiparametric MRI, the framework improved preoperative IDH classification beyond clinical variables and showed calibration and decision curve benefit. Independent prognostic value of the habitat signature suggests that spatial habitat architecture encodes biologically meaningful heterogeneity, providing an interpretable imaging bridge between glioma molecular status, microenvironmental organization, and survival risk.

Previous studies have predicted IDH status using whole-tumor radiomics, deep learning, or ROI-level habitat analysis [22-26]. However, these approaches may insufficiently characterize spatial heterogeneity and provide limited interpretability. Although MRI habitat studies based on perfusion, ADC, or diffusion kurtosis have demonstrated differences between IDH-mutant and IDH-wildtype gliomas [10, 27-31] , most rely on

hard clustering or global feature extraction, potentially obscuring voxel-scale variation and reducing cross-patient comparability [27, 29, 31, 32]. In contrast, our framework combined sliding-window radiomics mapping with Gaussian mixture model-based probabilistic clustering to generate continuous habitat probability maps [16]. This strategy achieved strong external performance without deep learning and yielded interpretable spatial heterogeneity and tumor–edema gradient metrics.

Interpretability analysis showed that IDH prediction was mainly driven by perfusion- and diffusion-related heterogeneity. Influential features included CBF- and ADC-derived entropy metrics and spatial measures such as Moran's I, fragmentation, and Gini coefficient. CBF reflects perfusion, angiogenesis, and microvascular remodeling, whereas ADC is associated with cellular density and microstructure [33]. Previous studies reported higher perfusion in IDH-wildtype gliomas and supported ADC as an imaging biomarker for IDH classification [34, 35]. Our findings extend these observations by suggesting that IDH-related phenotypes are reflected by voxel-wise spatial heterogeneity beyond mean perfusion or diffusion values. Entropy and Gini coefficient quantify phenotype diversity and imbalance, whereas Moran's I and fragmentation describe spatial autocorrelation and subregional disorganization, potentially capturing vascular, cellular, and infiltrative variation [28, 29, 36].

Peritumoral edema contained molecular and prognostic information. Prior dynamic susceptibility contrast perfusion habitat analyses identified infiltrative and vasogenic edema subregions with rCBV differences associated with IDH status and prognosis [28]. Multimodal studies similarly showed that subregions characterized by vascular

permeability and cellular density reflect microenvironmental heterogeneity and correlate with progression and survival [29]. Consistent with these findings, the superior performance of tumor–edema differential features suggests that contrast between tumor core and peritumoral edema adds information beyond tumor-only analysis [37].

Patients classified as high risk had significantly poorer overall survival, and the habitat signature remained independently associated with survival after adjustment for age, KPS, MGMT promoter methylation status, and EOR. This association remained robust after adjustment for CNS WHO grade or standard treatment, suggesting that voxel-wise habitat architecture adds prognostic value beyond established clinical, molecular, pathological, and treatment variables. Prior studies have linked perfusion- and diffusion-defined habitats to treatment resistance and survival [38], while multimodal MRI habitat analyses suggest that subregions with distinct vascular permeability and cellular density may reflect hypoxia, metabolic stress, and aggressive tumor microenvironments [29]. Thus, the habitat signature may complement clinical and treatment-related variables.

Several limitations should be acknowledged. First, the median follow-up was 26 months, and the low-risk survival estimate may be affected by censoring; longer follow-up is required. Second, the retrospective design may introduce selection bias because inclusion required complete multiparametric MRI and molecular data. Third, although IDH prediction was externally validated, survival analysis was limited to a subset of the external validation cohort and lacked independent multicenter validation. Fourth,

the habitat pipeline may be influenced by preprocessing, segmentation quality, and acquisition heterogeneity, despite ComBat harmonization and external validation. Prospective multicenter studies should confirm its robustness and clinical utility.

5 Conclusions

Multiparametric MRI-based voxel-wise probabilistic habitat modeling characterizes tumor and peritumoral heterogeneity, supports preoperative IDH prediction, and provides prognostic information for survival risk stratification in glioma.

6 Reference

1. Greenwald AC, Darnell NG, Hoefflin R, et al (2024) Integrative spatial analysis reveals a multi-layered organization of glioblastoma. Cell 187:2485-2501.e26. DOI:10.1016/j.cell.2024.03.029
2. Weller M, Wen PY, Chang SM, et al (2024) Glioma. Nat Rev Dis Primers 10:33. DOI:10.1038/s41572-024-00516-y
3. Gupta P, Dang M, Oberai S, et al (2024) Immune landscape of isocitrate dehydrogenase-stratified primary and recurrent human gliomas. Neuro Oncol 26:2239-2255. DOI:10.1093/neuonc/noae139
4. Zhang L, Fritah S, Nazarov PV, Kaoma T, Van Dyck E (2023) Impact of IDH Mutations, the 1p/19q Co-Deletion and the G-CIMP Status on Alternative Splicing in Diffuse Gliomas. Int J Mol Sci 24. DOI:10.3390/ijms24129825
5. Hu LS, Hawkins-Daarud A, Wang L, Li J, Swanson KR (2020) Imaging of intratumoral heterogeneity in high-grade glioma. Cancer Lett 477:97-106. DOI:10.1016/j.canlet.2020.02.025
6. Chen C, Du X, Yang L, et al (2023) Research on application of radiomics in glioma: a bibliometric and visual analysis. Front Oncol 13:1083080. DOI:10.3389/fonc.2023.1083080
7. Hajri R, Nicod-Lalonde M, Hottinger AF, Prior JO, Dunet V (2023) Prediction of Glioma Grade and IDH Status Using (18)F-FET PET/CT Dynamic and Multiparametric Texture Analysis. Diagnostics (Basel) 13. DOI:10.3390/diagnostics13152604
8. van der Voort SR, Incekara F, Wijnenga MMJ, et al (2023) Combined molecular subtyping, grading, and segmentation of glioma using multi-task deep learning. Neuro Oncol 25:279-289. DOI:10.1093/neuonc/noac166
9. Niu W, Yan J, Hao M, et al (2025) MRI transformer deep learning and radiomics for predicting IDH wild type TERT promoter mutant gliomas. NPJ Precis Oncol 9:89. DOI:10.1038/s41698-025-00884-y
10. Liu Y, Wang P, Wang S, et al (2023) Heterogeneity matching and IDH prediction in adult-type diffuse gliomas: a DKI-based habitat analysis. Front Oncol 13:1202170. DOI:10.3389/fonc.2023.1202170
11. Qiao J, Wu H, Liu J, et al (2023) Spectral Analysis Based on Hemodynamic Habitat Imaging Predicts Isocitrate Dehydrogenase Status and Prognosis in High-Grade Glioma. World Neurosurg 175:e520-e530. DOI:10.1016/j.wneu.2023.03.136
12. Beig N, Patel J, Prasanna P, et al (2018) Radiogenomic analysis of hypoxia pathway is predictive

of overall survival in Glioblastoma. Sci Rep 8:7. DOI:10.1038/s41598-017-18310-0
13. Sottoriva A, Spiteri I, Piccirillo SG, et al (2013) Intratumor heterogeneity in human glioblastoma reflects cancer evolutionary dynamics. Proc Natl Acad Sci U S A 110:4009-14. DOI:10.1073/pnas.1219747110
14. Hu LS, Ning S, Eschbacher JM, et al (2017) Radiogenomics to characterize regional genetic heterogeneity in glioblastoma. Neuro Oncol 19:128-137. DOI:10.1093/neuonc/now135
15. Zhang HM, Huo XB, Wang HL, Wang C (2022) Diagnostic Performance of Dynamic Susceptibility Contrast-Enhanced Perfusion-Weighted Imaging in Differentiating Recurrence From Radiation Injury in Postoperative Glioma: A Meta-analysis. J Comput Assist Tomogr 46:938-944. DOI:10.1097/rct.0000000000001356
16. Bernatowicz K, Grussu F, Ligero M, Garcia A, Delgado E, Perez-Lopez R (2021) Robust imaging habitat computation using voxel-wise radiomics features. Sci Rep 11:20133. DOI:10.1038/s41598-021-99701-2
17. Antonelli M, Poliani PL (2022) Adult type diffuse gliomas in the new 2021 WHO Classification. Pathologica 114:397-409. DOI:10.32074/1591-951x-823
18. Isensee F, Schell M, Pflueger I, et al (2019) Automated brain extraction of multisequence MRI using artificial neural networks. Hum Brain Mapp 40:4952-4964. DOI:10.1002/hbm.24750
19. Isensee F, Jaeger PF, Kohl SAA, Petersen J, Maier-Hein KH (2021) nnU-Net: a self-configuring method for deep learning-based biomedical image segmentation. Nat Methods 18:203-211. DOI:10.1038/s41592-020-01008-z
20. Orlhac F, Frouin F, Nioche C, Ayache N, Buvat I (2019) Validation of A Method to Compensate Multicenter Effects Affecting CT Radiomics. Radiology 291:53-59. DOI:10.1148/radiol.2019182023
21. Akiba T, Sano S, Yanase T, Ohta T, Koyama M (2019) Optuna: A Next-generation Hyperparameter Optimization Framework. ACM
22. Peng H, Huo J, Li B, et al (2021) Predicting Isocitrate Dehydrogenase (IDH) Mutation Status in Gliomas Using Multiparameter MRI Radiomics Features. J Magn Reson Imaging 53:1399-1407. DOI:10.1002/jmri.27434
23. Zhang H, Fan X, Zhang J, et al (2023) Deep-learning and conventional radiomics to predict IDH genotyping status based on magnetic resonance imaging data in adult diffuse glioma. Front Oncol 13:1143688. DOI:10.3389/fonc.2023.1143688
24. Wu J, Xu Q, Shen Y, Chen W, Xu K, Qi XR (2022) Swin Transformer Improves the IDH Mutation Status Prediction of Gliomas Free of MRI-Based Tumor Segmentation. J Clin Med 11. DOI:10.3390/jcm11154625
25. Yuan Y, Yu Y, Chang J, et al (2023) Convolutional neural network to predict IDH mutation status in glioma from chemical exchange saturation transfer imaging at 7 Tesla. Front Oncol 13:1134626. DOI:10.3389/fonc.2023.1134626
26. Stefano A (2024) Challenges and limitations in applying radiomics to PET imaging: Possible opportunities and avenues for research. Comput Biol Med 179:108827. DOI:10.1016/j.compbiomed.2024.108827
27. Kersch CN, Kim M, Stoller J, Barajas RF, Jr., Park JE (2024) Imaging Genomics of Glioma Revisited: Analytic Methods to Understand Spatial and Temporal Heterogeneity. AJNR Am J Neuroradiol 45:537-548. DOI:10.3174/ajnr.A8148
28. Wu H, Tong H, Du X, et al (2020) Vascular habitat analysis based on dynamic susceptibility contrast perfusion MRI predicts IDH mutation status and prognosis in high-grade gliomas. Eur Radiol 30:3254-

3265. DOI:10.1007/s00330-020-06702-2
29. Wang X, Xie Z, Wang X, et al (2025) Preoperative prediction of IDH genotypes and prognosis in adult-type diffuse gliomas: intratumor heterogeneity habitat analysis using dynamic contrast-enhanced MRI and diffusion-weighted imaging. Cancer Imaging 25:11. DOI:10.1186/s40644-025-00829-5
30. Yang Z, Lin R, Wu Z, et al (2025) Habitat subregions analysis based on neurite orientation dispersion and density imaging enhances isocitrate dehydrogenase genotyping in glioma. BMC Med Imaging 25:384. DOI:10.1186/s12880-025-01934-4
31. Zheng WY, Yang RH, Wan ZF, et al (2025) MRI-based habitat radiomics for preoperatively predicting IDH status in gliomas. Neurosurg Focus 59:E4. DOI:10.3171/2025.5.focus25135
32. Han Y, Wang Y, Cui W, Xiu S, Yang Y, Zhang J (2026) IDH Mutation Classification in Nonenhancing Gliomas: A Comparison of Habitat and Whole-Tumor Transfer Learning Strategies. J Magn Reson Imaging 63:1079-1089. DOI:10.1002/jmri.70187
33. Kim M, Kim HS (2016) Emerging Techniques in Brain Tumor Imaging: What Radiologists Need to Know. Korean J Radiol 17:598-619. DOI:10.3348/kjr.2016.17.5.598
34. van Santwijk L, Kouwenberg V, Meijer F, Smits M, Henssen D (2022) A systematic review and meta-analysis on the differentiation of glioma grade and mutational status by use of perfusion-based magnetic resonance imaging. Insights Imaging 13:102. DOI:10.1186/s13244-022-01230-7
35. Bhatti F, Strobel J, Tench C, et al (2025) Apparent diffusion coefficient for genetic characterization of untreated adult gliomas: A meta-analysis stratified by methods. Neurooncol Adv 7:vdaf103. DOI:10.1093/noajnl/vdaf103
36. Singh G, Manjila S, Sakla N, et al (2021) Radiomics and radiogenomics in gliomas: a contemporary update. British Journal of Cancer 125:641-657. DOI:10.1038/s41416-021-01387-w
37. Wang H, Zeng L, Wu H, et al (2024) Preoperative vascular heterogeneity based on dynamic susceptibility contrast MRI in predicting spatial pattern of locally recurrent high-grade gliomas. Eur Radiol 34:1982-1993. DOI:10.1007/s00330-023-10149-6
38. Li C, Yan JL, Torheim T, et al (2019) Low perfusion compartments in glioblastoma quantified by advanced magnetic resonance imaging and correlated with patient survival. Radiother Oncol 134:17-24. DOI:10.1016/j.radonc.2019.01.008

7 Statements & Declarations

7.1 Ethics approval and consent to participate

This retrospective study was conducted in accordance with the ethical standards of the Declaration of Helsinki and was approved by the Ethics Review Board of the XXX Hospital of XXX (Ethics Number: XXXXXX). The requirement for written informed consent from participants was waived by the approving ethics committee due to the retrospective nature of the study.

7.2 Consent for publication

The need for written informed consent was waived with the confirmation of patient data confidentiality by the institutional Ethics Committee for this retrospective study.

7.3 Availability of data and materials

The data that support the findings of this study are not publicly available due to privacy or ethical restrictions, but are available on request from the corresponding author.

7.4 Competing interests

The authors declare that they have no competing interests.

7.5 Funding

This work was supported by Qinhuangdao S&T Plan Program (grant number: 202301A212)

7.6 Author Contributions

TZ: Conceptualization, Data curation, Formal analysis, Investigation, Visualization, Writing – original draft.
LY: Conceptualization, Data curation, Investigation, Validation, Writing – original draft.
DZ: Methodology, Validation, Writing – review and editing.
JD: Funding acquisition, Resources, Project administration.
QS: Software, Methodology, Formal analysis.
DL: Supervision, Conceptualization, Writing – review and editing.

7.7 Acknowledgments

Not applicable

7.8 Clinical trial number

Not applicable.

8 Figures

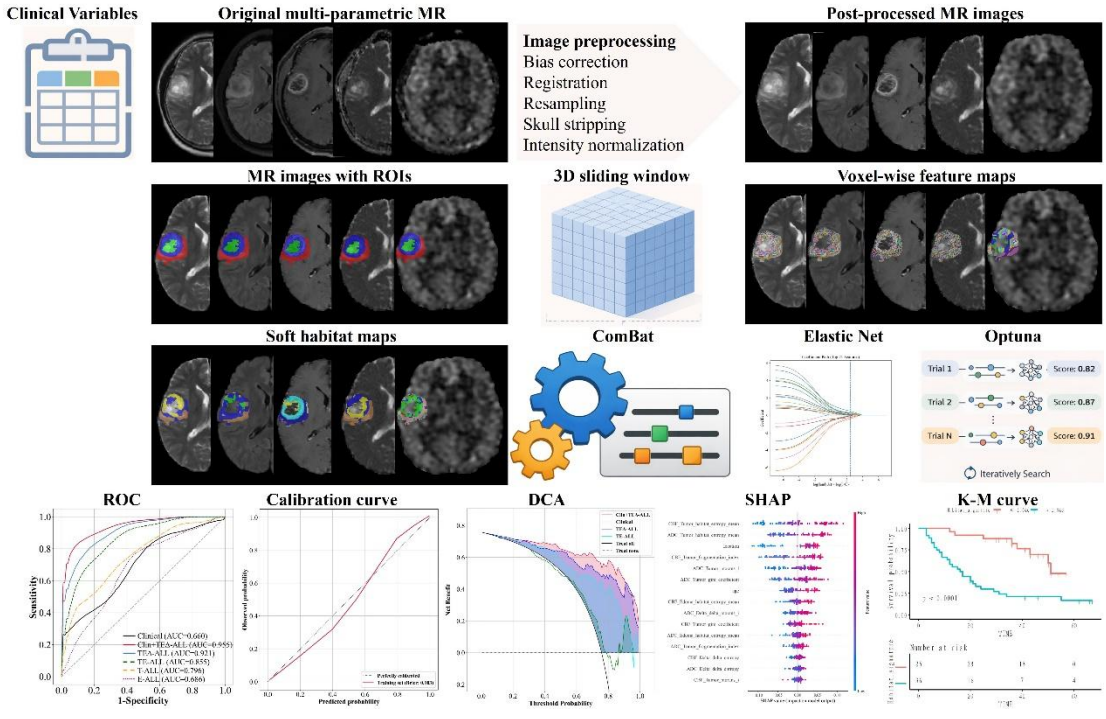


Figure 1. Overview of the proposed voxel-wise habitat modeling framework for

IDH prediction and survival analysis in diffuse glioma.

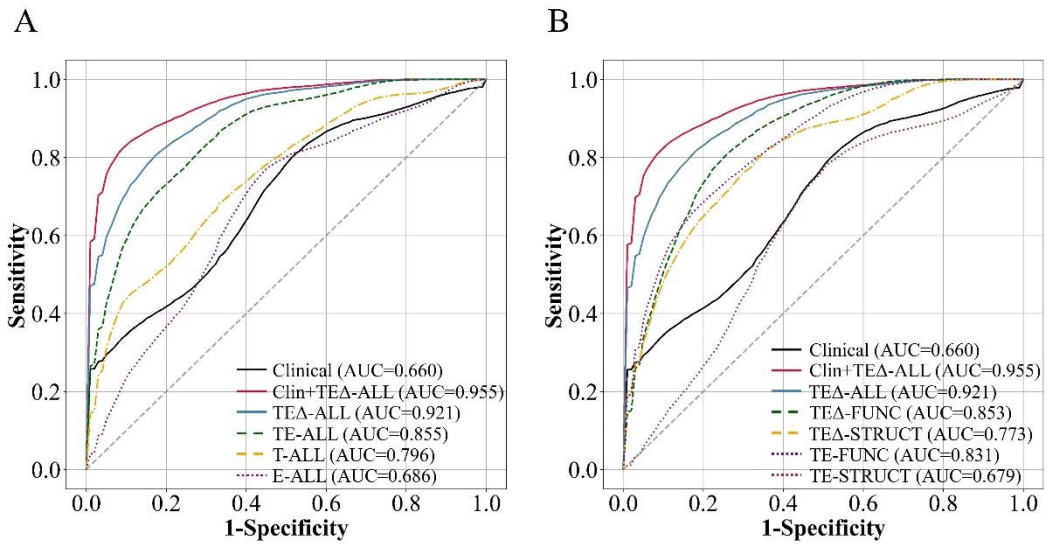


Figure 2. Receiver operating characteristic (ROC) curves of different predictive models for IDH status in the external validation cohort. (A) Comparison of habitat-based models constructed using different spatial regions. (B) Comparison of modality-based models, including functional imaging models and structural imaging models. Abbreviations: AUC, area under the receiver operating characteristic curve; T, tumor region; E, edema region; TE, combined tumor and edema regions; Δ, tumor–edema difference features; ALL, all radiomics habitat features; FUNC, functional imaging features (ADC and CBF); STRUCT, structural imaging features (T1CE, T2, and FLAIR).

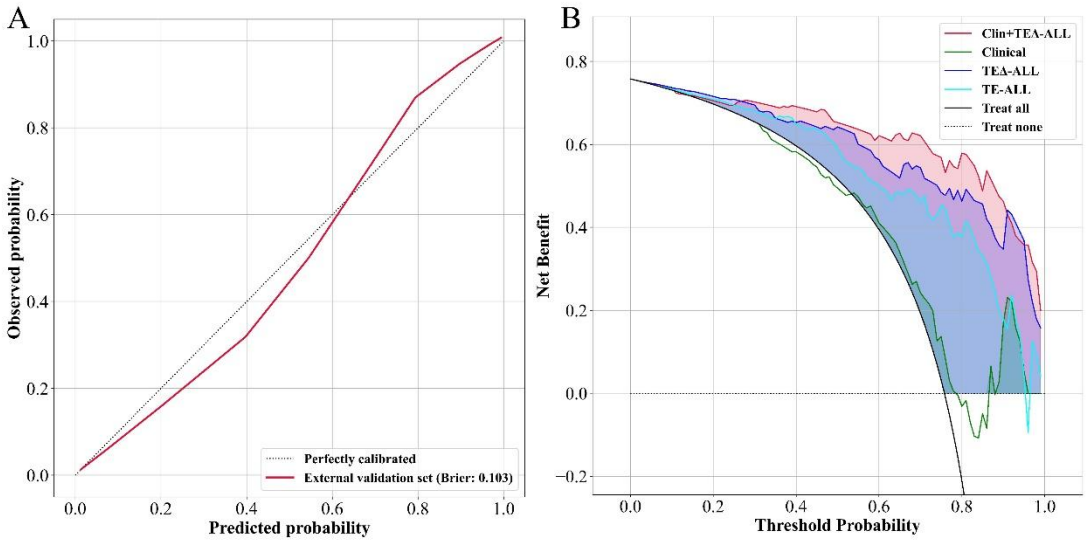


Figure 3. Calibration and clinical utility of the predictive models in the external validation cohort. (A) Calibration curve of the Clin+TE Δ -ALL model. **(B)** Decision curve analysis (DCA) comparing the net clinical benefit of different models across a range of threshold probabilities. Decision curve analysis is presented descriptively; uncertainty intervals for net benefit were not estimated. Abbreviations: DCA, decision curve analysis; TE, combined tumor and edema regions; Δ, tumor − edema difference features; ALL, all radiomics habitat features.

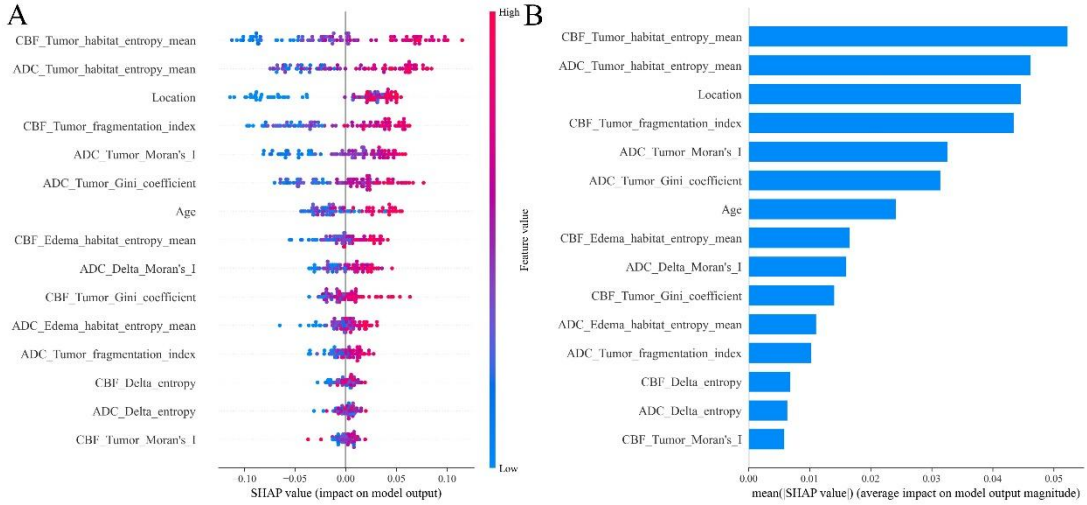


Figure 4. SHAP-based interpretability analysis of the Clin+TE Δ -ALL model. (A) SHAP summary (beeswarm) plot illustrating the impact of individual features on model

predictions. Each point represents a patient-level observation, with the horizontal axis indicating the SHAP value (i.e., the contribution of the feature to the model output). Feature values are color-coded from low (blue) to high (red). Features are ranked according to their overall importance. (B) Bar plot showing the mean absolute SHAP values of the top features, representing their average contribution to the model output magnitude.

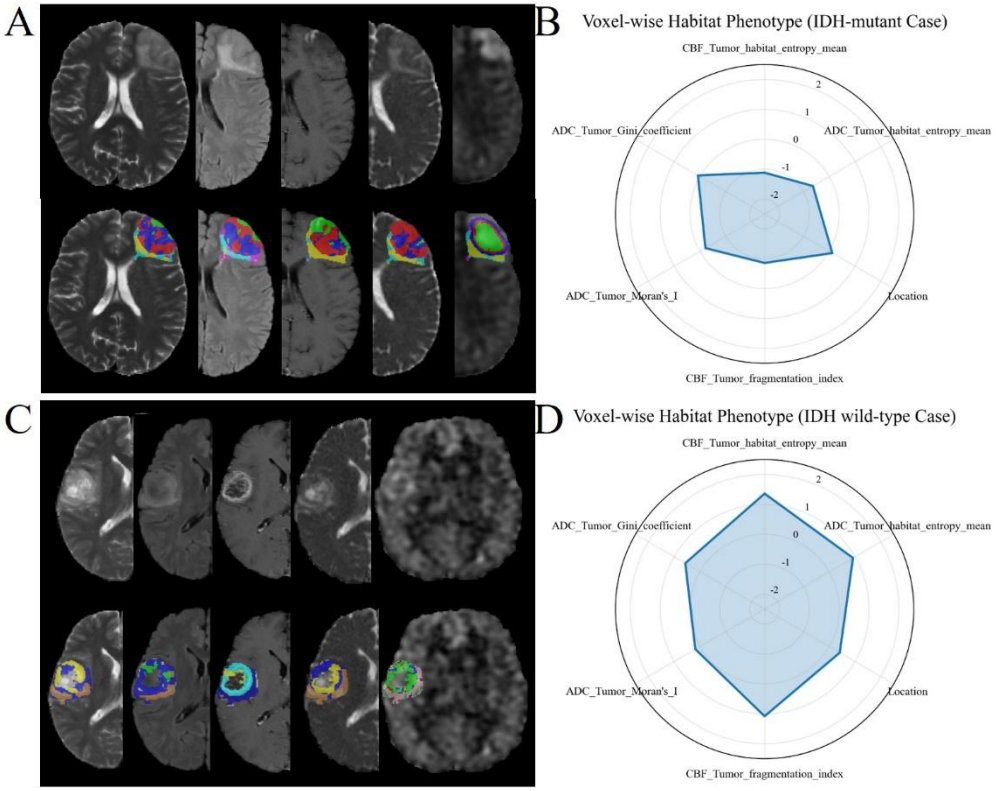


Figure 5. Representative voxel-wise habitat phenotypes for IDH- mutant and wildtype gliomas. (A, C) Representative multimodal MRI and corresponding voxel-wise habitat maps for two glioma cases with different IDH status. Images include axial T2WI, T2-FLAIR, T1CE, ADC, and CBF maps with corresponding habitat probability maps reconstructed within the tumor region. (A) A 45-year-old male patient with an IDH-mutant glioma in the left frontal lobe. (C) A 62-year-old female patient with an

IDH-wildtype glioma in the right temporal lobe. (B, D) Radar plots showing selected model-contributing variables normalized using training-set z scores. The IDH-mutant case showed lower values for several entropy and fragmentation-related habitat features, whereas the IDH-wildtype case showed higher habitat heterogeneity across these selected variables. These cases are illustrative and are not intended to represent the full cohort distribution.

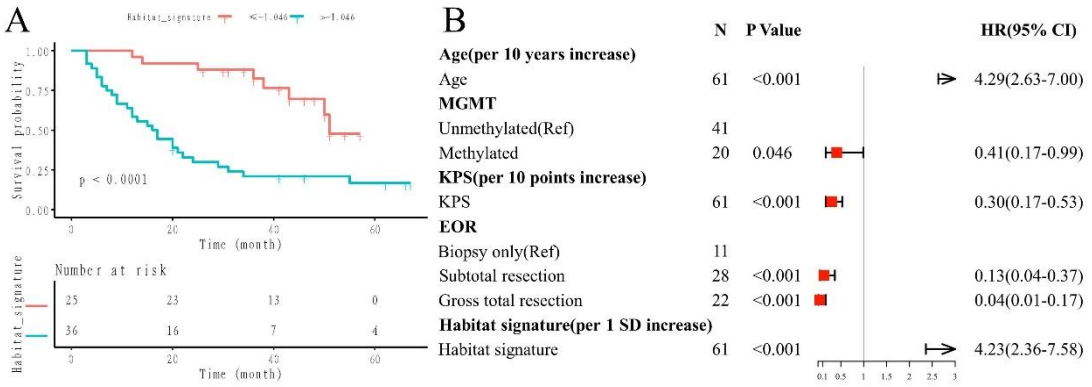


Figure 6. Survival analysis based on the habitat-derived risk signature. (A) Kaplan–Meier survival curves stratified by the habitat signature. (B) Forest plot of the multivariable Cox proportional hazards analysis for overall survival.

9 Tables

Table 1. Clinical characteristics of patients in different sets

Characteristic	Training set	External validation set	*P*
Sample size	174	95	
Age (year, mean±SD)	52.6± 17.7	54.5 ± 20.7	0.445
Sex (%)			>0.999
Female	70 (40.2%)	38 (40.0%)	
Male	104 (59.8%)	57 (60.0%)	
Location (%)			0.758
Frontal lobe	39 (22.4%)	17 (17.9%)	
Temporal	21 (12.1%)	13 (13.7%)	
Parietal/Occipital	16 (9.2%)	6 (6.3%)	
Other	33 (19.0%)	18 (18.9%)	
Multilobar (≥2 lobes)	65 (37.4%)	41 (43.2%)	
WHO CNS5 integrated			0.794

diagnosis (%)			
Astrocytoma, IDH-mutant, CNS WHO grade 2	14 (8.0%)	6 (6.3%)	
Astrocytoma, IDH-mutant, CNS WHO grade 3	10 (5.7%)	7 (7.4%)	
Astrocytoma, IDH-mutant, CNS WHO grade 4	8 (4.6%)	6 (6.3%)	
Glioblastoma, IDH-wildtype, CNS WHO grade 4	132 (75.9%)	72 (75.8%)	
Oligodendroglioma, IDH-mutant and 1p/19q-codeleted, CNS WHO grade 2	4 (2.3%)	3 (3.2%)	
Oligodendroglioma, IDH-mutant and 1p/19q-codeleted, CNS WHO grade 3	6 (3.4%)	1 (1.1%)	
IDH (%)			>0.999
Mutant	42 (24.1%)	23 (24.2%)	
Wild-type	132 (75.9%)	72 (75.8%)	

Note: Independent-samples t-test was used for continuous variables, and Pearson chi-square test or Fisher's exact test was used for categorical variables, as appropriate. The parietal/occipital group included tumors confined to either the parietal or occipital lobe. The other category comprised deep or midline structures, infratentorial regions, and peri-rolandic areas. Tumors involving two or more lobes were categorized as multilobar. CNS, central nervous system; IDH, isocitrate dehydrogenase; WHO, World Health Organization; WHO CNS5, 2021 World Health Organization Classification of Tumors of the Central Nervous System, fifth edition; 1p/19q-codeleted, combined deletion of chromosome arms 1p and 19q.

Supplementary Files

This is a list of supplementary files associated with this preprint. Click to download.

- Supplementary.docx